Lagrangian versus Eulerian spectral estimates of surface kinetic energy over the global ocean

Xinwen Zhang[1], Xiaolong Yu[1], Aurélien L. Ponte[2], Zoé Caspar-Cohen[2,3], Sylvie Le Gentil[2], Lu Wang[2], Wenping Gong[1]

[1]School of Marine Sciences, Sun Yat-sen University, and Southern Marine Science and Engineering Guangdong Laboratory (Zhuhai), Zhuhai, China
[2]Ifremer, Université de Brest, CNRS, IRD, Laboratoire d'Océanographie Physique et Spatiale, IUEM, Brest, France
[3]Scripps Institution of Oceanography, University of California, San Diego, La Jolla, California, USA

Key Points:

- Surface kinetic energy spectral distributions and levels are compared in a global realistic numerical simulation.
- Lagrangian spectra are smoother than Eulerian counterparts at all major frequency peaks.
- Adequate frequency bandwidths are needed to match Lagrangian and Eulerian estimates of kinetic energy levels.

Corresponding author: Xiaolong Yu, `yuxlong5@mail.sysu.edu.cn`

Abstract

Geographical distributions and frequency content of ocean surface kinetic energy (KE) are estimated in a 1/48° high-resolution global numerical model of the ocean circulation. Eulerian (fixed-point) KE rotary frequency spectra and band-integrated energy levels (e.g., low-frequency, tidal and near-inertial) are considered as references which are compared to Lagrangian (along-flow) estimates. Eulerian and Lagrangian KE exhibit broad qualitative similarities with dominance of low-frequency motions and presence of distinct spectral peaks at semidiurnal, near-inertial, and diurnal frequencies. One notable difference is that, apart for the near-inertial band, Lagrangian spectra are systematically smoother, e.g., with wider and lower spectral peaks compared to Eulerian counterparts. Nevertheless, no significant differences are found between Lagrangian and Eulerian global KE levels provided adequate frequency bandwidths are chosen. Our findings demonstrate that Lagrangian observations of the Global Drifter Program have great potential to accurately map global KE variability at high frequencies (e.g., tidal and near-inertial).

Plain Language Summary

Ocean surface currents play a pivotal role in the transport of heat and energy over the global ocean, and thus affect global climate patterns and marine ecosystems. Ocean currents are inherently a multi-scale system, which requires for instance to decompose and describe the flow at different temporal scales. Much of the rapid (high frequency) ocean variability is not known accurately at the moment. Here, we show that the information brought by the displacements of surface drifters about ocean currents may help fill this gap. This is demonstrated with global ocean numerical models, which are now able to represent high-frequency variability such as associated with tides, winds and eddies, and are therefore powerful tools to evaluate ocean multi-scale variability. We compare here fixed-point (i.e., "Eulerian") and along-flow (i.e., "Lagrangian" or drifter) kinetic energy estimates. Our results show that these two different perspectives can be reconciled in the estimation of energy levels, as long as adequate frequency bandwidths are chosen to account for distortions of rapid motion signals in the Lagrangian frame of reference. This work highlights the potential of drifter-based observations in enhancing our understanding of high-frequency ocean variability.

1 Introduction

The ocean circulation controls the transport and distribution of physical properties and biochemical tracers across the global ocean. Ocean motions at spatial scales smaller than several hundreds of kilometers and temporal scales shorter than months account for a dominant fraction of kinetic energy (KE; Ferrari & Wunsch, 2009). Its two main contributors are quasi-geostrophic balanced motions, which include mesoscale eddies (spatial scales of 20-300 km, periods of weeks to months) and submesoscale motions (spatial scales of 0.2-20 km, periods of hours to days), and unbalanced internal gravity waves (spatial scales <300 km and periods <1 day). Mesoscale eddies account for most of the ocean KE and play a key role in the physical equilibrium and biogeochemical functioning of the ocean at climatic scales (McWilliams, 2008; McGillicuddy et al., 2007; Treguier et al., 2014). Submesoscale motions induce, on the other hand, a vigorous vertical circulation and determine the vertical exchanges of heat, carbon, and nutrients (McWilliams, 2016; Lévy et al., 2018; Taylor & Thompson, 2023). Internal gravity waves are a major driver for turbulent mixing in the ocean, which is fundamental component of the global overturning circulation (Whalen et al., 2020). Internal waves are commonly organized around frequency, and are observed to have energy peaks at tidal and near-inertial frequencies, and a continuous energy distribution across higher frequencies, commonly known as the internal wave continuum.

Provided sufficient information is available along spatial and temporal dimensions, one way of characterizing balanced and unbalanced motions is to estimate the distribution of surface KE as function of spatial and temporal scales. Torres et al. (2018) examined for instance the distribution of surface KE in wavenumber-frequency space from a high resolution numerical simulation, and showed that lower frequency motions emanate from larger scales and spread to finer spatial and temporal scales. The emergence of wide-swath altimetry and surface current measuring satellite missions has fostered efforts aiming at improving our understanding of oceanic variability down to O(10 km) and of its manifestation on satellite and in situ observations (Morrow et al., 2019; Du et al., 2021).

An emerging dataset to proceed with in situ observational descriptions across scales is that of the Global Drifter Program (GDP; Elipot et al., 2016). Yu et al. (2019) compared frequency spectra estimated from GDP drifter data (i.e., Lagrangian) and output from a high-resolution Massachusetts Institute of Technology general circulation model (MITgcm) simulation (i.e., Eulerian), which enable to point towards inaccurate representations of tidal and near-inertial variability in the numerical model. Arbic et al. (2022) performed a similar yet more detailed comparison based on Yu et al. (2019) datasets and an additional global tide-resolving simulation of the HYbrid Coordinate Ocean Model (HYCOM). In global maps and zonal averages, numerical models captured the low-frequency and high-frequency variance qualitatively. HYCOM simulation, because of its more frequently updated wind-forcing and a more finely tuned implementation of tidal variability, was found closer to GDP drifter values compared to MITgcm simulation. However, both studies questioned the equivalence between Eulerian and Lagrangian estimates, which has not been demonstrated yet. At tidal frequencies, Caspar-Cohen et al. (2022) recently demonstrated that the displacement of surface drifters may distort low-mode internal tide signals which translated to wider spectral peaks, a mechanism coined “apparent incoherence”.

In this work, we compare Lagrangian and Eulerian spectral decompositions of surface KE at global scale, with the aid of output from a high-resolution ocean numerical model (LLC4320 simulation; Yu et al., 2019). A key question addressed here is whether Eulerian high-frequency KE levels can be recovered from drifter (Lagrangian) observations. The paper is organized as follows. Section 2 describes the LLC4320 simulation, the Lagrangian numerical simulation experiments, and methods of spectral analysis and energy level estimates. Comparisons between Eulerian and Lagrangian KE fields are described in section 3. Discussions and conclusions are given in sections 4 and 5, respectively.

2 Materials and Methods

2.1 LLC4320 simulation

The LLC4320 simulation was performed using MITgcm (Marshall et al., 1997) on a global Latitude-Longitude-polar Cap (LLC) grid (Forget et al., 2015) for a period of 14 months between 10 September 2011 and 15 November 2012. The model has a horizontal grid spacing of 1/48° (approximately 2.3 km at the equator and 0.75 km in the Southern Ocean), and thereby resolves mesoscale eddies and permits submesoscale variability. The model time step was 25 seconds, and model variables were stored at hourly intervals. The model was forced by 6-hourly surface flux fields (including 10-m wind velocity, 2-m air temperature and humidity, downwelling long- and short-wave radiation, and atmospheric pressure load) from the ECMWF operational reanalysis, and included the full lunisolar tidal constituents that are applied as additional atmospheric pressure forcing. The LLC4320 uses a flux-limited monotonicity-preserving (seventh order) advection scheme, and the modified Leith scheme of Fox-Kemper and Menemenlis (2008) for horizontal viscosity. The K-profile parameterization (Large et al., 1994) is used for vertical viscosity and diffusivity. In this study, we use a yearlong record of the instantaneous surface fields at every hour, starting on 15 November 2011.

2.2 Lagrangian experiments

Lagrangian simulations are performed with LLC4320 hourly surface velocity outputs and the ‘Parcels’ python package (Lange & Van Sebille, 2017; Delandmeter & Van Sebille, 2019). Surface virtual drifters are initially released every 50 grid points of LLC4320 grid (about 50 to 100 km spacing), and drifter positions and velocity fields are stored at hourly rate. The Lagrangian simulation is about one year long (from 15 November 2011 to 9 November 2012). Virtual drifters are released every 10 days at initial release positions if no virtual drifter is present within a radius equal to the distance to closest neighbor at initial release. This continuous seeding enables to maintain a continuous coverage throughout the Lagrangian simulation. The number of virtual drifters is of about 60,000 at the start, and reaches about 95,000 drifters at the end of the simulation. The Lagrangian particles in the LLC4320 simulation (i.e., virtual drifters) are scattered throughout the open ocean worldwide (Figure S1 in Supporting Information), and their spatial distribution is broadly in line with that of GDP drifters over the global ocean albeit with an instantaneous drifter density larger by about two orders of magnitudes (Elipot et al., 2016; Yu et al., 2019). Heavily sampled regions concentrate in flow convergence zones (e.g., the interior of subtropical gyres). In contrast, areas of flow divergence (e.g., the equatorial region, upwelling areas) as well as polar and coastal regions are generally less sampled. As a result, the number of 60-day particle trajectory segments at midlatitudes (30°-60°N and S) is at least a factor of 2 larger than that in the equatorial region (10°S-10°N).

2.3 Frequency rotary spectrum and bandwidth selection for energy integration

For Eulerian estimates, hourly surface horizontal velocity time series are used to compute rotary spectra of horizontal velocity at each model grid point. For Lagrangian estimates, rotary spectra are computed from horizontal velocities along particle trajectories. For both datasets, we first divide velocity time series into segments of 60 days overlapping by 50% and linearly detrend over each segment, and then compute the 1D discrete Fourier transform of complex-valued fields ($u + iv$, where u and v are zonal and meridional velocity, respectively) multiplied by a Hanning window. Spectra are formed by multiplying Fourier amplitudes by their complex conjugates and averaged over time for Eulerian estimates and according to segment mean drifter's latitudes and longitudes for Lagrangian estimates (Figure S1 in Supporting Information). Given the geographical distribution of particle trajectories, velocity data in polar regions with latitude higher than 60° and in coastal waters with depth shallower than 500 m or sampling numbers smaller than 5 are not considered in the calculation for both datasets.

Rotary frequency spectral densities are integrated over four frequency bands to compute KE components of interest, including high-frequency (>0.5 cpd, absolute values here and hereinafter), semidiurnal, near-inertial, diurnal bands. Total KE is estimated from temporal averages of instantaneous velocity fields, and low-frequency KE is computed as total KE minus high-frequency KE. We examine the sensitivity of the regression coefficient and root mean square errors between Eulerian and Lagrangian semidiurnal, near-inertial and diurnal KE energy levels to different frequency bandwidths of integration (Figure S2 in Supporting Information). For semidiurnal band, the closest match between Eulerian and Lagrangian energy levels is achieved for the ±0.3 cpd bandwidth with a regression coefficient value closest to unity and a root mean square error plateauing at approximately 10^{-3} m^2 s^{-2} (equivalent to 15.6% of the averaged Eulerian semidiurnal energy level). In contrast, for diurnal and near-inertial bands, the narrowest bandwidth (i.e., ±0.1 cpd) yields the best comparison based on the two metrics. Consequently, the semidiurnal, near-inertial, diurnal bands are respectively defined as 1.7-2.3 cpd, 0.9-1.1f and 0.9-1.1 cpd, where f is the Coriolis frequency.

To achieve a balance between drifter density and spatial variability of bin-averaged diagnostics, a bin size of 1° latitude is employed to compare Eulerian and Lagrangian zonally averaged rotary spectra and associated band integrals. For global maps, the band-integrated KE estimates are averaged in 1°× 1° spatial bins. Finally, following Arbic et al. (2022), we compute the ratio of Lagrangian KE divided by the sum of Lagrangian and Eulerian KE.

Note that a ratio of 0.5 indicates equality between Lagrangian KE and Eulerian KE, a ratio exceeding 0.5 indicates Lagrangian KE overestimates Eulerian KE, and a ratio below 0.5 indicates Lagrangian KE underestimates Eulerian KE.

3 Results

Lagrangian and Eulerian zonally averaged spectra both show expected peaks at low frequencies, near-inertial and tidal frequencies (Figures 1a-b). Along with Figures 1c-d, Lagrangian spectral peaks appear to be systematically broader and weaker than Eulerian ones, consistent with a spreading of energy. This spreading is clear around main tidal peaks and increases with frequency such that Lagrangian higher frequency tidal constituents (e.g. 3 cpd, 4 cpd, ...) are hardly noticeable unlike Eulerian ones. The ratio of Lagrangian to Eulerian spectra consistently indicates that Lagrangian peak values at tidal frequencies are lower but wider than Eulerian ones (Figure 1c). This is consistent with the findings of Zaron and Elipot (2021), which noted that the drifter tidal peaks do not stand out above the background spectrum as strongly as in tide model predictions. Caspar-Cohen et al. (2022) consistently demonstrated that the distortion of tidal internal waves induced by surface drifter motions, a process coined as apparent incoherence, leads to broader tidal peaks.

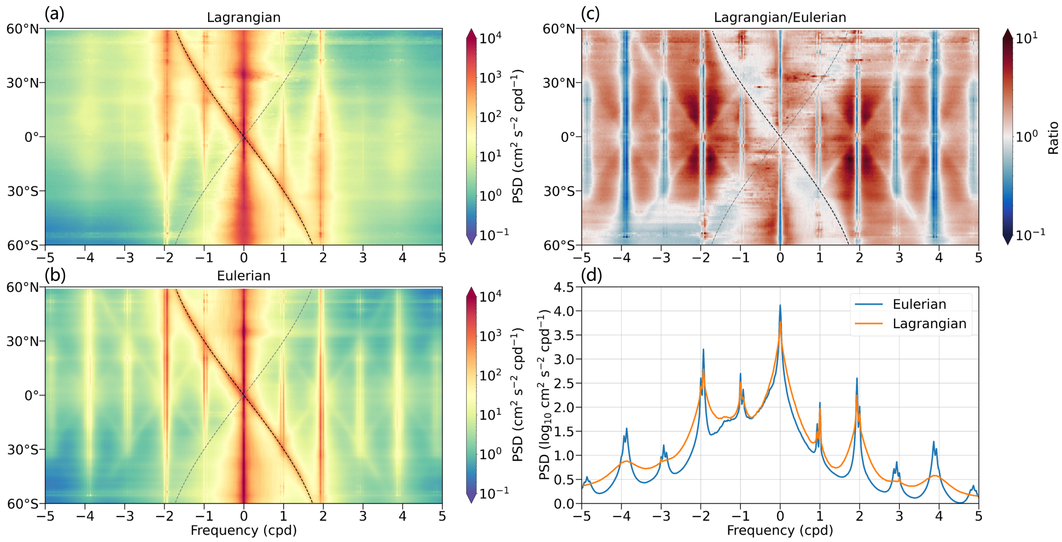

Figure 1. Zonally averaged rotary frequency spectra in 1° latitude bins from (a) Lagrangian and (b) Eulerian horizontal velocity fields at the surface layer and (c) their ratio, with positive (negative) frequencies corresponding to counterclockwise (clockwise) rotating motions, which are cyclonic (anticyclonic) in the Northern Hemisphere. The cyclonic Coriolis frequency ($f/2\pi$ cpd) is indicated by the gray dashed line and the anticyclonic inertial frequency ($-f/2\pi$ cpd) is indicated by the black dashed line. (d) Globally averaged anticyclonic (at negative frequencies) and cyclonic (at positive frequencies) spectra of the Eulerian (blue) and Lagrangian (orange) horizontal velocity fields.

At subinertial frequencies, a similar mechanism may be invoked to explain the smoothing of the low-frequency energy peak of energy in Lagrangian diagnostics: Lagrangian particles sample both spatial and temporal variability, which leads to shorter velocity decorrelation timescales and broader spectra (Middleton, 1985; Davis, 1983; Lumpkin et al., 2002; LaCasce, 2008). At near-inertial frequencies, the smoothing of the peak is not visible in latitude dependent spectra (Figures 1a-b), and the ratio of Lagrangian to Eulerian spectra indicates values close to unity (Figure 1c). This suggests that drifter displacements do not distort the signature of near-inertial waves similarly to internal tides. Another obvious contrast is that energy levels at the anticyclonic frequencies are substantially higher than those at the cyclonic frequencies, particularly below the semidiurnal frequency band (Figure 1d). This is consistent with the natural polarization of internal gravity waves which leads to a ratio between cyclonic and anticyclonic kinetic energies that scales as $(\omega + f)/(\omega - f)$ (Gill, 1982), where ω is the frequency.

3.1 Zonally-averaged kinetic energy

Zonally averaged low-frequency, semidiurnal, near-inertial, diurnal KE estimated from Eulerian and Lagrangian velocity time series are shown in Figure 2. Eulerian and Lagrangian estimates show great visual similarities overall. Low-frequency KE dominates total energy and its variations along latitude therefore mimic total KE variations (Figure S4 in Supporting Information). Low-frequency energy peaks near the equator, at 35°N and 55°S at the locations of Northern Hemisphere western boundary currents and the Antarctic Circumpolar Current respectively (Figure 2a). At 35°N, Lagrangian energies overestimate Eulerian ones, which will be argued to partly result from the unequal sampling of high vs low energy regions (Davis, 1985) and may be mitigated with alternative geographical binning (see Discussion section). Lagrangian zonally averaged semidiurnal KE is visually slightly lower than Eulerian KE at almost all low and mid latitudes (Figure 2b). In contrast, Lagrangian zonally averaged near-inertial KE follow Eulerian estimates relatively well over most latitudes, except for a clear underestimation at 30°S (Figure 2c). For the diurnal KE, discrepancies are relatively larger, with a 15.4% difference in average (Figure 2d), compared to low-frequency (7%), semidiurnal (11.1%), and near-inertial (6.7%) bands. There are two substantial mismatches between Eulerian and Lagrangian diurnal KE, one is in 20°N, which may be associated with the less Lagrangian particles in Luzon strait, and one is in 30°S, in line with the underestimate in near-inertial KE.

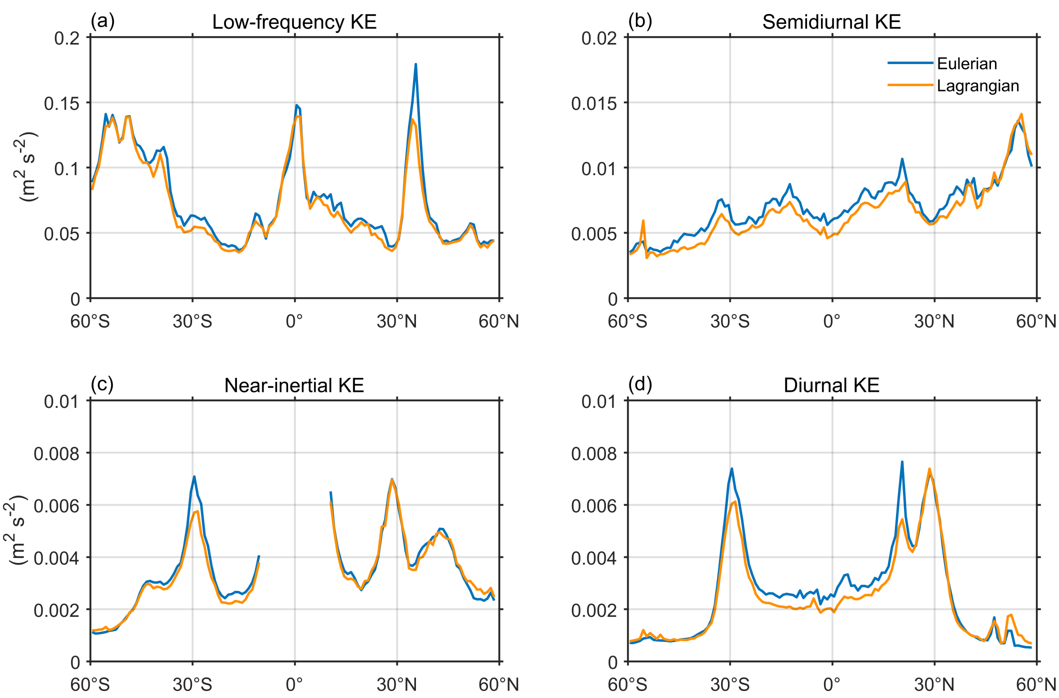

Figure 2. Zonally averaged (a) low-frequency, (b) semidiurnal, (c) near-inertial and (d) diurnal KE in 1° latitude bins estimated from Eulerian velocity field (blue) and Lagrangian particle trajectories with binning (orange).

3.2 Low-frequency kinetic energy maps

Global maps of low-frequency KE highlight prominent large-scale currents and energetic areas, including equatorial and western boundary currents such as the Gulf Stream and the Antarctic Circumpolar Current (Figures 3a-b). Lagrangian and Eulerian KE are in good visual agreement, with a mean value and standard deviation of the energy ratio about 0.49 and 0.07, respectively (Figure 3c). A noticeable difference is that Lagrangian energies appear smoother than Eulerian ones around large-scale current features, which presumably results from the spatial advection of Lagrangian drifter over the temporal window of energy integration. This smoothing also reflects on energy ratios. Nearby energetic current features, Lagrangian energy thus tends to underestimate Eulerian energy maxima in the core of these features (ratio below 0.5) and overestimate Eulerian energy on the surroundings (ratio above 0.5). Akin to the low-frequency maps, Eulerian and Lagrangian global maps of total KE exhibit broadly similar magnitudes and spatial distributions, although Eulerian diagnostics reveal finer structures in regions of high KE (Figure S3 in Supporting Information).

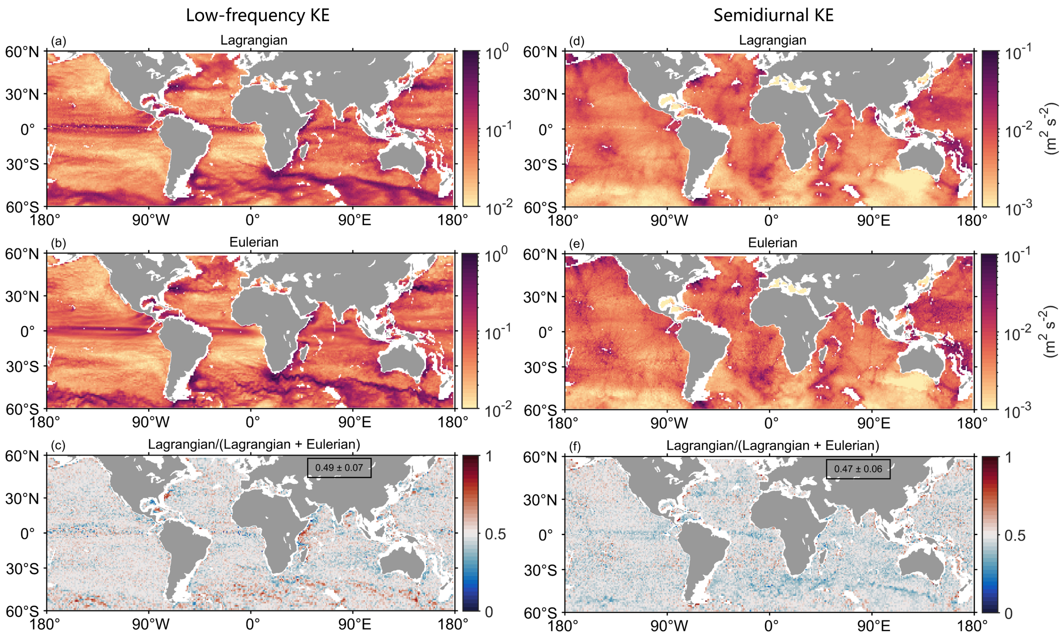

Figure 3. (a-c) Global maps of Lagrangian and Eulerian low-frequency KE at the surface layer and the ratio of Lagrangian KE/(Lagrangian KE+Eulerian KE) in 1°× 1° bins. (d-f) Same as (a-c) but for semidiurnal KE. The mean value of the ratio and one standard deviation are indicated in (c) and (f).

3.3 High-frequency kinetic energy maps

Surface semidiurnal, near-inertial and diurnal KE are all an order of magnitude smaller than low-frequency KE. The comparison between Lagrangian and Eulerian semidiurnal KE estimates show significant similarities globally (Figures 3d-e). Both clearly display hotspots of internal tide generation, e.g., near Hawaii islands, the French Polynesian islands, the Aleutians island chain, 40°S and 40°N in the Atlantic as well as the western Pacific. The discrepancies at semidiurnal frequencies are relatively larger compared to low frequencies, with a mean energy ratio of 0.47 and standard deviation of 0.06. Noticeable differences between Lagrangian and Eulerian energies occur near coastal areas, where the Lagrangian field may exhibit semidiurnal KE levels considerably larger than the Eulerian field. This overestimate is likely to result from Lagrangian particles crossing continental shelves, where tidal currents are faster, over the 60-day window of energy integration. By contrast, Lagrangian semidiurnal energies systematically underestimate semidiurnal KE over open ocean areas. This underestimation may indicate the bandwidth tuned based on a global criterion may not be be sufficient in these areas to account for the smearing of the semidiurnal tidal spectral peak (Figure 1d).

Lagrangian and Eulerian estimates of near-inertial KE show particularly similar spatial patterns across the global ocean (Figures 4a-b). Intensified near-inertial KE generally occurs at mid latitudes, with largest values concentrated in the North Pacific. This is broadly in line with storm-track regions and spatial distribution of wind work (Alford, 2003). Expected enhancements also occur at ±30° latitudes where the local inertial frequency coincides with diurnal frequencies. Nearly meridionally oriented beams appear in the low to mid latitudes and are particularly evident in the Eulerian field, likely associated with individual tropical cyclones and storms in the model forcing fields. The mean value and standard deviation of the energy ratio are 0.49 and 0.07, respectively (Figure 4c). Differences between Eulerian and Lagrangian near-inertial KE are modest in global maps compared to those within semidiurnal and diurnal bands. Nonetheless, Lagrangian energy slightly underestimates near-inertial KE over open ocean regions in the Southern Hemisphere, around 30°S. It is probably related to the influence of diurnal bands and an change in the nature of motions (larger contribution from internal tides for instance).

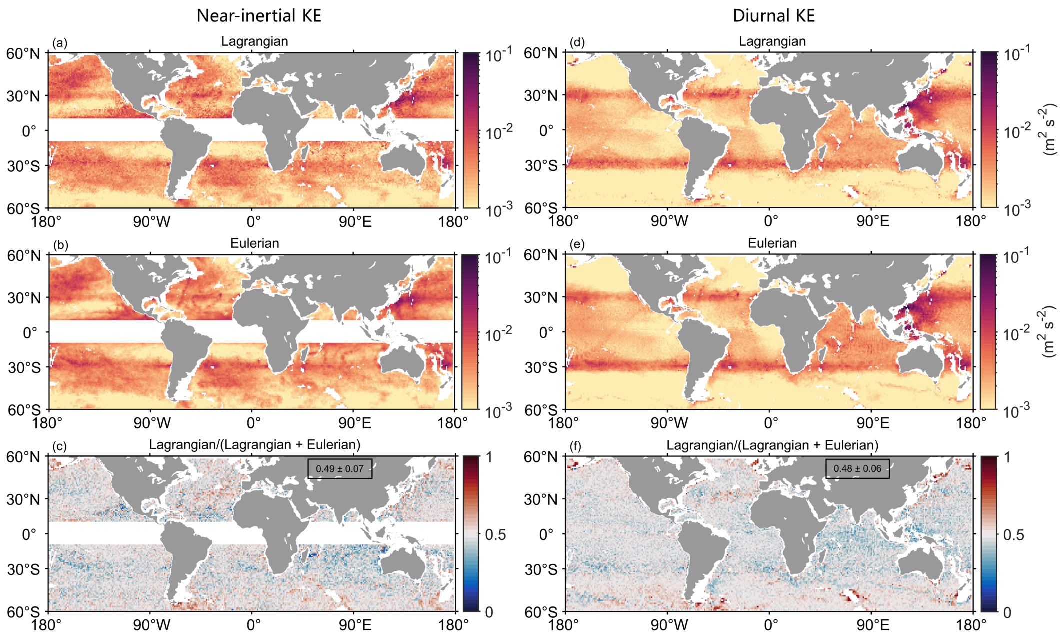

Figure 4. (a-c) Global maps of Lagrangian and Eulerian near-inertial KE at the surface layer and the ratio of Lagrangian KE/(Lagrangian KE+Eulerian KE) in 1°× 1° bins. (d-f) Same as (a-c) but for diurnal KE. The mean value of the ratio and one standard deviation are indicated in (c) and (f).

For the diurnal band, the global map of Lagrangian KE also closely reproduces the Eulerian KE visually (Figures 4d-e). The most prominent feature of diurnal KE is the enhancement around ±30° latitudes, where the diurnal wind-forcing (sea breeze) aligns with the local inertial frequency. Similar to the semidiurnal band, the Lagrangian field shows larger values than the Eulerian field in several coastal regions (Figure 4f). These coastal regions are mostly located outside 30°S and 30°N, where diurnal internal tides are not expected to freely propagate, indicating that their differences may be caused by barotropic tides or trapped baroclinic tides. Another non-trivial distinction is that the Lagrangian particles underestimate the strength of diurnal KE in the Luzon strait (approximately 20°N). Apparent incoherence is in general expected to be weaker at diurnal frequencies than at semidiurnal frequencies, due to the larger horizontal wavelength of diurnal tides (Caspar-Cohen et al., 2022). The strength of the low-frequency flow may counteract this general tendency here.

4 Discussion

In previous studies, ocean surface KE in high-resolution global simulations has been compared with KE from GDP surface drifters (Yu et al., 2019; Arbic et al., 2022). Model-drifter comparisons showed good qualitative over a wide range of frequency bands but systematic discrepancies were also observed, and the pending question is whether these discrepancies could be attributed to Lagrangian/Eulerian biases. Taking the comparison between the LLC4320 simulation and GDP drifters for example, a deficit of low-frequency energy within the equatorial region was observed, with energy peak values reaching 0.15 $m^2\ s^{-2}$ for the model and 0.34 $m^2\ s^{-2}$ for GDP drifters (Yu et al., 2019). Their difference (approximately 0.2 $m^2\ s^{-2}$) is one order of magnitude larger than the Lagrangian-Eulerian difference near the equator (which is of order $10^{-2}\ m^2\ s^{-2}$ as shown in Figure 2a). Moreover, Yu et al. (2019) reported that the LLC4320 simulation exhibits KE four times higher in the semidiurnal band and three times lower in the near-inertial band compared with GDP drifter data. However, the global mean ratios of Lagrangian KE to Lagrangian KE+Eulerian KE obtained in this study are 0.47±0.06 for the semidiurnal band (Figure 3f) and 0.49±0.07 for the near-inertial band (Figure 4c), both of which are close to 0.5. This means that, on average, Lagrangian KE is nearly equal to Eulerian KE in the LLC4320 simulation. Therefore, our results suggest that Lagrangian/Eulerian biases are very likely not the main cause of the model-drifter discrepancies.

Arbic et al. (2022) identified the sensitivity of the Lagrangian semidiurnal energy estimate to the bandwidth of integration, which the present study corroborates. This sensitivity arises from apparent incoherence which leads to a widening of the semidiurnal tidal peak (Caspar-Cohen et al., 2022). A single common value (i.e., 1.7-2.3 cpd) for the bandwidth of integration that produced the best match between Lagrangian and Eulerian energy estimates was chosen in the present study. However, the bandwidth of integration may not be the same for Eulerian and Lagrangian energy diagnostics. Limiting bandwidth may be desirable in order to mitigate contamination from the background energy spectrum. Given the sharper shape of Eulerian semidiurnal peaks, smaller bandwidths may be afforded for Eulerian diagnostics. The width of Eulerian semidiurnal peaks is related to internal tide incoherent timescales, whose geographical variations may lead to geographically varying choices for the bandwidth of integration of Eulerian energy. Caspar-Cohen et al. (2022) theoretically predict that the intensity of apparent incoherence and thus the associated widening of the Lagrangian spectrum depends on parameters that may vary geographically such as the low-frequency energy level or internal tide properties (wavenumber, incoherent timescale). The bandwidth of integration of Lagrangian estimates may thus be modulated geographically in order again to mitigate contamination from the background energy spectrum. Such more advanced choices for bandwidth of energy integration would be good material for future studies, even though the present study indicates this would be mostly relevant for the semidiurnal band which exhibits most sensitivity to integration bandwidth.

Lastly, we examine the sensitivity to particle spatial distribution by comparing zonally averaged Lagrangian KE estimated from trajectories with ("2D binned") and without ("raw") spatial binning (Figure S4 in Supporting Information). On average, raw Lagrangian energy estimates tend to underestimate Eulerian energy , likely due to the preferential sampling of low-energy regions by Lagrangian particles (Freeland et al., 1975). The deficit caused by the inhomogeneous sampling of Lagrangian particles, in KE levels of up to 20%, can be compensated by averaging Lagrangian diagnostics in longitude/latitudes bins. Our recommendation is to geographically bin energy estimates prior to integration over larger domains (e.g., zonally, globally) to mitigate such sampling biases. However, it should be noted that along a similar line but at the bin level, the combination of spatio-temporal inhomogeneities and energy variability within individual bins may also lead to systematic differences between Eulerian and Lagrangian estimates (Davis, 1991), such as those observed nearby large current systems. The role of such sampling bias in explaining observed differences has not been investigated here but could constitute an interesting follow up study. Further, we have chosen here a 60-day time window for spectral decompositions and energy estimates, and this choices induces spatial smoothing compared to Eulerian estimates. Above-mentioned study may be useful in order to identify whether statistical techniques enabling more local (temporally and therefore spatially for drifters) estimates of high-frequency energy levels should be devised.

5 Summary

The goal of this study is to quantify the relationship between Eulerian and Lagrangian KE spectral content and its geographical variability. A practical objective is to assess the extent to which Lagrangian particles can estimate Eulerian KE levels. To achieve this, we have compared the surface KE estimated using the LLC4320 global ocean model, and the Lagrangian simulations performed by the LLC4320 hourly surface velocity output. Our main findings are summarized as follows:

1) A common feature among all dominant frequency bands is that Lagrangian spectra appear smoothed compared to Eulerian ones. This smoothing is least in near-inertial band and most pronounced in semidiurnal and low-frequency bands. At low frequencies, this smoothing is attributed to the simultaneous sampling of spatial and temporal variability by drifters and associated decrease in the decorrelation timescale (Middleton, 1985; LaCasce, 2008). The widening of the semidiurnal peak is consistent with the mechanism of apparent incoherence. The relatively minor difference between the Lagrangian and Eulerian near-inertial frequency peaks remains to be explained.

2) With a tuned choice of bandwidth of integration, good agreements for semidiurnal, near-inertial and diurnal KE can be achieved between Eulerian and Lagrangian simulations. This implies that Lagrangian particles advected by Eulerian filed can qualitatively reproduce the original Eulerian high-frequency variance. Compared to Eulerian estimates, Lagrangian estimates are more sensitive to bandwidth, as expected from their character of broadened spectral peaks. Particularly, Lagrangian semidiurnal tides are featured with a wider bandwidth than other high-frequency motions. We have identified avenues to refine further this choice of bandwidth of integration.

GDP drifter observations have been extensively used in many previous studies focusing on low-frequency and mesoscale oceanic flows (Lumpkin & Johnson, 2013; Lumpkin, 2016). Our findings confirm further that the drifter data may provide an estimate of high-frequency variance, such as tidal and near-inertial motions. Drifter and model differences, as showed in Yu et al. (2019) and Arbic et al. (2022), are not mainly caused by Lagrangian vs Eulerian sampling nature. This work may motivate future studies on particular aspects of the model-observation and model-model discrepancies, and is a substantial step towards the production of high frequency KE climatologies.

Acknowledgments

This work was funded by grants from the National Natural Science Foundation of China (Grants 42206002, 42361144844), and Guangdong Basic and Applied Basic Research Foundation (2023A1515010654). This work was also supported by ANR project 17-CE01-0006-01 entitled EQUINOx (Disentangling Quasi-geostrophic Motions and Internal Waves in High Resolution Satellite Observations of the Ocean).

Open Research

The LLC4320 simulation output is available at https://data.nas.nasa.gov/ecco/data.php.

References

Alford, M. H. (2003). Redistribution of energy available for ocean mixing by long-range propagation of internal waves. *Nature*, *423*(6936), 159-162.

Arbic, B. K., Elipot, S., Brasch, J. M., Menemenlis, D., Ponte, A. L., Shriver, J. F., ... Nelson, A. D. (2022). Near-surface oceanic kinetic energy distributions from drifter observations and numerical models. *Journal of Geophysical Research: Oceans*, *127*(10), e2022JC018551.

Caspar-Cohen, Z., Ponte, A., Lahaye, N., Carton, X., Yu, X., & Gentil, S. L. (2022). Characterization of internal tide incoherence: Eulerian versus lagrangian perspectives. *Journal of Physical Oceanography*, *52*(6), 1245-1259.

Davis, R. E. (1983). Oceanic property transport, lagrangian particle statistics, and their prediction. *Journal of Marine Research*, *41*, 163-194.

Davis, R. E. (1985). Drifter observations of coastal surface currents during CODE: The statistical and dynamical views. *Journal of Geophysical Research: Oceans*, *90(C3)*, 4756-4772.

Davis, R. E. (1991). Observing the general circulation with floats. *Deep Sea Research Part A. Oceanographic Research Papers*, *38*, S531-S571.

Delandmeter, P., & Van Sebille, E. (2019). The Parcels v2.0 Lagrangian framework: new field interpolation schemes. *Geoscientific Model Development*, *12*(8), 3571-3584.

Du, Y., Dong, X., Jiang, X., Zhang, Y., Zhu, D., Sun, Q., ... Peng, S. (2021). Ocean surface current multiscale observation mission (OSCOM): Simultaneous measurement of ocean surface current, vector wind, and temperature. *Progress in Oceanography*, *193*, 102531.

Elipot, S., Lumpkin, R., Perez, R. C., Lilly, J. M., Early, J. J., & Sykulski, A. M. (2016). A global surface drifter data set at hourly resolution. *Journal of Geophysical Research: Oceans*, *121*(5), 2937-2966.

Ferrari, R., & Wunsch, C. (2009). Ocean circulation kinetic energy: Reservoirs, sources, and sinks. *Annual Review of Fluid Mechanics*, *41*, 253-282.

Forget, G., Campin, J. M., Heimbach, P., Hill, C. N., Ponte, R. M., & Wunsch, C. (2015). Ecco version 4: an integrated framework for non-linear inverse modeling and global ocean state estimation. *Geoscientific Model Development*, *8*(10), 3071-3104.

Fox-Kemper, B., & Menemenlis, D. (2008). Can large eddy simulation techniques improve mesoscale rich ocean models? In *Ocean modeling in an eddying regime* (p. 319-337). American Geophysical Union (AGU).

Freeland, H. J., Rhines, P. B., & Rossby, T. (1975). Statistical observations of the trajectories of neutrally buoyant floats in the north atlantic. *Journal of Marine Research*, *33*.

Gill, A. E. (1982). Atmosphere-ocean dynamics. *Academic press*.

LaCasce, J. H. (2008). Lagrangian statistics from oceanic and atmospheric observations. In J. B. Weiss & A. Provenzale (Eds.), *Transport and mixing in geophysical flows: Creators of modern physics* (pp. 165–218). Springer Berlin Heidelberg.

Lange, M., & Van Sebille, E. (2017). Parcels v0.9: Prototyping a lagrangian ocean analysis framework for the petascale age. *Geoscientific Model Development*, *10*(11), 4175-4186.

Large, W. G., Mcwilliams, J. C., & Doney, S. C. (1994). Oceanic vertical mixing - a review and a model with a nonlocal boundary-layer parameterization. *Reviews of Geophysics*, *32*(4), 363-403.

Lumpkin, R. (2016). Global characteristics of coherent vortices from surface drifter trajectories. *Journal of Geophysical Research-Oceans*, *121*(2), 1306-1321.

Lumpkin, R., & Johnson, G. C. (2013). Global ocean surface velocities from drifters: Mean, variance, el nino-southern oscillation response, and seasonal cycle. *Journal of Geophysical Research: Oceans*, *118*(6), 2992-3006.

Lumpkin, R., Treguier, A.-M., & Speer, K. (2002). Lagrangian eddy scales in the northern atlantic ocean. *Journal of Physical Oceanography*, *32*(9), 2425-2440.

Lévy, M., Franks, P. J. S., & Smith, K. S. (2018). The role of submesoscale currents in structuring marine ecosystems. *Nature Communications*, *9*.

Marshall, J., Adcroft, A., Hill, C., Perelman, L., & Heisey, C. (1997). A finite-volume, incompressible navier stokes model for studies of the ocean on parallel computers. *Journal of Geophysical Research: Oceans*, *102*(C3), 5753-5766.

McGillicuddy, D. J., Anderson, L. A., Bates, N. R., Bibby, T., Buesseler, K. O., Carlson, C. A., … Steinberg, D. K. (2007). Eddy/wind interactions stimulate extraordinary mid-ocean plankton blooms. *Science*, *316*(5827), 1021-1026.

McWilliams, J. C. (2008). The nature and consequences of oceanic eddies. In *Ocean modeling in an eddying regime* (p. 5-15). American Geophysical Union (AGU).

McWilliams, J. C. (2016). Submesoscale currents in the ocean. *Proceedings of the Royal Society a-Mathematical Physical and Engineering Sciences*, *472*(2189).

Middleton, J. F. (1985). Drifter spectra and diffusivities. *Journal of Marine Research*, *43*, 37-55.

Morrow, R., Fu, L. L., Ardhuin, F., Benkiran, M., Chapron, B., Cosme, E., … Zaron, E. D. (2019). Global observations of fine-scale ocean surface topography with the surface water and ocean topography (SWOT) mission. *Frontiers in Marine Science*, *6*, 232.

Taylor, J. R., & Thompson, A. F. (2023). Submesoscale Dynamics in the Upper Ocean. *Annual Review of Fluid Mechanics*, *55*, 103–127.

Torres, H. S., Klein, P., Menemenlis, D., Qiu, B., Su, Z., Wang, J. B., … Fu, L. L. (2018). Partitioning ocean motions into balanced motions and internal gravity waves: A modeling study in anticipation of future space missions. *Journal of Geophysical Research: Oceans*, *123*(11), 8084-8105.

Treguier, A. M., Deshayes, J., Le Sommer, J., Lique, C., Madec, G., Penduff, T., … Talandier, C. (2014). Meridional transport of salt in the global ocean from an eddy-resolving model. *Ocean Science*, *10*(2), 243-255.

Whalen, C. B., de Lavergne, C., Garabato, A. C. N., Klymak, J. M., MacKinnon, J. A., & Sheen, K. L. (2020). Internal wave-driven mixing: governing processes and consequences for climate. *Nature Reviews Earth & Environment*, *1*, 606-621.

Yu, X., Ponte, A. L., Elipot, S., Menemenlis, D., Zaron, E. D., & Abernathey, R. (2019). Surface kinetic energy distributions in the global oceans from a high-resolution numerical model and surface drifter observations. *Geophysical Research Letters*, *46*(16), 9757-9766.

Zaron, E. D., & Elipot, S. (2021). An assessment of global ocean barotropic tide models using geodetic mission altimetry and surface drifters. *Journal of Physical Oceanography*, *51*(1), 63-82.